

DETAILED SPECTRAL ANALYSIS OF THE 260 K SEC XMM-Newton DATA OF 1E 1207.4-5209 AND SIGNIFICANCE OF A 2.1 keV ABSORPTION FEATURE

Kaya Mori¹, James C. Chonko² and Charles J. Hailey²
 kaya@cit.utoronto.ca, chonko@astro.columbia.edu, chuckh@astro.columbia.edu

Draft version March 26, 2019

ABSTRACT

We have done a reanalysis of the 260 ksec XMM-Newton observation of 1E 1207.4-5209 described in Bignami et al. (2003) and De Luca et al. (2004). We find no evidence for a third or fourth feature in the spectrum, which had been interpreted as higher harmonics of a cyclotron line. Only the two broad absorption features previously reported are statistically significant (Sanwal et al. 2002), Hailey & Mori (2002)). We identify the origins of the overestimate of the significance of the third and fourth spectral lines. As first pointed out by Protopassov et al. (2002) the F-statistic in the case of a line search cannot be described by the standard F-distribution even asymptotically, as assumed in the previous analyses. Therefore no valid conclusions can be drawn from these analyses. We calculate the finite statistics F-distribution and show that with this correct distribution the third and fourth lines are not significant. We compare this with two additional statistical tests, one line model dependent and the other independent. Our continuum fits have significantly lower² ($\chi^2 / \nu = 1$) than earlier work, and this is true for a much broader range of physically plausible models than were previously investigated. This further reduced the significance of the extra lines. We explicitly fit the insignificant residuals around 2.1 keV. For those models where the weak residuals are strongest, we find them at an instrument AlM edge, and not at a statistically distinct energy, in contrast to earlier studies. This is true not only for the model favored in earlier investigations, but for all reasonable continuum models. Previous analyses also addressed the instrumental artifact issue by studying the 3C 273 AlM edge residuals and demonstrating that the feature in 1E 1207 is too strong to be associated with a AlM edge. We show this conclusion results from an overestimate of the continuum near the AlM edge.

Subject headings: stars: neutron { X-rays { individual: 1E 1207.4-5209 { methods: statistical

1. introduction

The study of thermal emission from isolated neutron stars (INS) is a clean way to probe neutron star physics since the surface emission is uncontaminated by the strong emission from an accretion disk. In particular, many INS (age 10^3 – 10^5 yrs) are good candidates because the surface is sufficiently hot for the thermal emission to be observed and not obscured by non-thermal emission in the magnetosphere. The spectral signature in thermal spectra is an excellent diagnostic tool to probe the strong magnetic field and gravity on the surface.

Two broad absorption features were discovered in the INS 1E 1207 by Chandra (Sanwal et al. 2002) and later confirmed by XMM-Newton (Mereghetti et al. 2002). The discovery was followed by the detection of a single spectral feature in the X-ray thermal spectra of three nearby INS (Haberl et al. 2003; van Kerkwijk et al. 2004; Haberl et al. 2004). 1E 1207 still remains unique because it shows more than one spectral feature as opposed to the other three INS which only show a single absorption feature.

However, the identification of spectral features in NS thermal spectra is not straightforward because of a variety of effects such as magnetic field, gravity and unknown surface composition. Soon after the discovery of spectral features in the 1E 1207 spectrum several different interpretations were proposed ranging from Helium atomic lines at $B = 10^{14}$ G (Sanwal et al. 2002), Iron atomic lines at $B = 10^{12}$ G (Mereghetti et al. 2002) and Oxygen/Neon

atomic lines at $B = 10^{12}$ G (Hailey & Mori 2002; Mori & Hailey 2003). Recently, Bignami et al. (2003) (hereafter B03) proposed electron cyclotron lines as the origin based on the detection of two additional absorption features at 2.1 and 2.8 keV in the 260 ksec XMM-Newton observations. They interpreted these four absorption lines as the fundamental and three harmonics of cyclotron lines. De Luca et al. (2004) (hereafter DL04) re-analyzed the same XMM-Newton data and also found that the 3rd and 4th feature are significant.

In this paper we present our detailed analysis of the same 260 ksec XMM-Newton observations and investigate the significance of the two additional absorption features at 2.1 keV and 2.8 keV. The paper is structured in the following fashion. In x2 we describe our data reduction methodology. In x3 we discuss the best-fit models which describe the two lower energy line features and global continuum, and which serve as a basis for assessing the need for additional components to describe the putative 2.1 keV and 2.8 keV features. x4 is the heart of the paper, where we discuss variance statistical methodologies for assessing the presence of weak lines and apply multiple approaches to determine the reality of the two spectral features. In x5 we discuss the phase-resolved data. In x6 we discuss the internal consistency of the MOS and PN data and establish, through analysis of the residuals at the putative line positions, that these weak features are instrumental artifacts. In x7 we present our conclusions.

¹ Canadian Institute for Theoretical Astrophysics, 60 St. George St., Toronto, ON, Canada, M5S 3H8

² Columbia Astrophysics Laboratory, 550 W. 120th St., New York, NY 10027

2. data reduction methodology

XM M -Newton observed the IN S 1E 1207 for two full orbits starting on August 4, 2002. The PN camera was operated with a thin filter in the "small window" mode. This allows accurate timing of the source photons (6 ms time resolution) and minimizes pile up. The two MOS cameras were operated in the "full frame" mode with a thin filter. We processed the 260 ksec XM M -Newton data using SAS version 5.4.1. We used canned response matrices for all the instruments and generated ancillary files by the SAS command "arfgen." The total exposure time for PN and MOS after removing time intervals with high background counts are 156 ksec and 231 ksec respectively.

We extracted the source photons from a 45" radius circle centered on the source for all cameras. There are sufficient photons in the PN camera to enable selection of only single events to achieve the best spectral resolution. Most of our results are based on this higher quality singles data, however later we discuss some results from the doubles analysis. The MOS cameras have less photons so we used all events in our analysis to improve the photon statistics. This is permissible because the larger MOS pixel size leads to fewer split events.

Background regions were carefully selected according to the recommendations of the XM M -Newton calibration team.³ In the PN camera we chose a 45" radius circle background region the same distance from the readout node as the source region to ensure similar noise. An annular background region encircling the source was not used to avoid out-of-time events from the source. In the MOS cameras we used a circular region away from the source according to the calibration team recommendations. However we also tried an annular region surrounding the source and found no significant deviations in the continuum fit parameters. The source is located in a supernova remnant and non-uniform X-ray emission from the remnant could influence the neutron star spectra. To validate our choice of background region we chose three different background regions for each instrument and compared the spectral fit parameters of the source did not significantly change with our choice of background region.

The spectra were rebinned such that each bin contained at least 40 counts and analyzed using XSPEC v11.3.1 in the 0.3{4.0 keV energy range. We adopted the energy band between 0.3 and 4.0 keV for the PN instrument. For the MOS instruments we selected the 0.5{4.0 keV band because the MOS is not well-calibrated at lower energies. Continuum fit parameters for the PN and MOS instruments were in good agreement.

The long XM M -Newton observation permits splitting the full observation in order to search for time variability. We split the observation into four approximately equal time intervals and found no deviations between the four observations. They yielded statistically consistent continuum fit parameters. We conclude that there was no time dependence during the total observation and therefore we use the data from the entire observation for all subsequent analysis.

3. analysis of data using continuum models

3.1. Introduction

In this section we consider fits to the global 1E 1207 spectra using a variety of physically motivated spectral models. Most of these models are not compatible with the data and are rejected. For those models which provide good fits to the data we determine the relevant fitting parameters. Our best models have much improved² over the previous work. This drastically decreases the potential significance of any third or fourth features in the 1E 1207 spectra. Nevertheless the issue of properly fitting additional spectral features is a complex one, and we postpone addressing it until x4. Here we only set the stage by providing information on the best fit continuum models.

3.2. Atmosphere models for neutron star thermal spectra

NS atmosphere models are sensitive to the assumed surface composition. The surface of a NS can be, in principle, any element between Hydrogen and Iron, because only $10^{-19} M_{\odot}$ of material is required to make an optically thick atmosphere (Romani 1987). The presence of an atmosphere will distort the spectral energy distribution (SED) from a Planckian shape, as will the presence of a magnetic field. For $B = 0$, hydrogen atmosphere models have the hardest spectrum due to the steep drop-off of the free-free absorption cross-section with increasing energy. Studies on heavy element atmospheres show that numerous atomic lines and edges are present due to dominant bound-bound or bound-free opacities and thus the SED is close to black-body (Romani 1987). In general, X-ray spectra become softer (closer to black-body) and show more discrete spectral features for heavier elements.

Magnetic field effects are also important for both discrete features and SED. Recent studies on a fully-ionized hydrogen atmosphere show that its SED becomes softer as magnetic field strength increases (Ho & Lai 2003). At $B > 10^{12}$ G, the electron binding energy (even for the hydrogen atom) can become a significant fraction of the surface temperature of an NS (0.1 keV). Thus the assumption of fully-ionized gas may not be valid even for a hydrogen atmosphere. Ho et al. (2003) constructed hydrogen atmosphere models by taking into account the contribution of neutral Hydrogen in the opacity and equation of state. They showed a magnetized hydrogen atmosphere is softened by opacity from bound species compared to a fully-ionized hydrogen atmosphere. For surface elements heavier than Hydrogen, non-magnetized atmosphere models show that the SED becomes softer with bound-bound and bound-free opacities dominating over free-free absorption and scattering.

From the above observations we conclude that realistic atmosphere models for 1E 1207 will have a SED somewhere between a blackbody and a magnetized fully-ionized hydrogen model. Our subsequent model fitting will reflect this full range of continuum models.

3.3. Description of models to the data (no third or fourth line assumed)

In the following few sections we describe our fit to the data without the assumption of a third or fourth line in

³ <http://xm.m.vilspa.esa.es/docs/documents/CAL-TN-0018-2-1.pdf>

the spectrum. Fits with such additional lines are discussed in §4. Therefore our "baseline" models always consist of the two universally accepted lines in the 1E 1207 spectrum, which we model as Gaussian absorption lines at 0.7 and 1.4 keV.

For each continuum component we adopt one of the following three physically plausible models; blackbody (BB), magnetized hydrogen atmosphere (HA) or power-law (PL). The magnetized hydrogen atmosphere model was constructed assuming a fully-ionized hydrogen atmosphere at $B = 10^{12}$ G, close to the dipole field strength as measured from the spin-down parameters (private communication with V.E. Zavlin). We also tried B -fields as low as $B = 0$ (Zavlin et al. 1996), and this did not alter the continuum parameters significantly. Higher B -fields ($> 4.4 \cdot 10^{13}$ G), just give results closer to the black-body case (Ho & Lai 2003).

In our fits to the spectrum we used one continuum component along with the two absorption lines. For all instruments the one-component models did not yield acceptable χ^2 values ($\chi^2 = 1.3 \{2.0\}$) and showed significant residuals above 2 keV. This strongly suggests the need for another continuum component to fit the high energy tail.

Given two continuum components and two absorption lines there are three types of continuum models defined as below. They consist of two continuum models (C1 and C2), and two absorption lines (L1 and L2). C1/L1 and C2/L2 refer to the lower and higher energy spectral component respectively. The three classes of models considered (with the notation C meaning line L resides on continuum component C)

$$\text{Model I: } C1 \quad L1 \quad L2 + C2$$

$$\text{Model II: } C1 \quad L1 + C2 \quad L2$$

$$\text{Model III: } (C1 + C2) \quad L1 \quad L2$$

For L1 and L2 the Gaussian absorption line was modeled as

$$F(E) / \exp(-\exp(-(E - E_0)^2 / 2w^2))g \quad (1)$$

where and w refer to the line depth and width. We fit other absorption line profiles such as a Lorentzian but the results were similar. DL04 fit asymmetric absorption lines profiles with two additional parameters. However this type of profile is not well-motivated. The exact shape of the absorption features may be asymmetric or have substructure from blended lines (Mori & Hailey 2003). Thus we chose simple Gaussian line shapes and to show fit residuals. When we fit photo-absorption edges to the two absorption features at 0.7 and 1.4 keV, the χ^2 was not as good as for the Gaussian lines in any of the continuum models.

3.3.1. Physical meaning of model I, II and III

Identification of spectral features in NS thermal spectra is not straightforward since the line parameters depend on various NS parameters such as surface element, ionization state, magnetic field strength and gravitational redshift (Hailey & Mori 2002; Mori & Hailey 2003). Therefore, it is important whether the observed spectral features originate from the same region or layer.

The presence of two continuum components complicates our interpretation of the observed absorption features. We assume that the two continuum components originate from

two different regions on the NS surface. For instance, C1 is emitted from a large area on the surface and C2 is emitted from a hot polar cap (DL04).

Model I assumes that L1 and L2 are from the same region as the emission of C1 and Model II assumes that they are from different regions. Model III assumes that L1 and L2 are from a layer above the two regions emitting continuum photons. Several physical models predicting a layer made of electron-positron or electron-ion pairs a few NS radii above the NS surface have been proposed (Fermi & Sturmer 1991; Wang et al. 1998; Ruderman 2003). Such a layer may become optically thick and modify the thermal spectra from the NS surface. In addition, absorption in model III can take place anywhere between the NS and the observer (e.g. magnetosphere, supernova remnant, ISM or materials of the XMM-Newton mirrors and cameras).

3.4. Results of continuum model fitting to XMM-Newton data

We searched for continuum models that are consistent with the data using models I, II and III as defined in the previous section. We emphasize that the set of models we considered is far more comprehensive than that of DL04 (§3.3). We considered all permutations of blackbody (BB), magnetized hydrogen atmosphere (HA) and power law (PL) models for C1 and C2.

All the two-component thermal models (and combinations of BB and HA) fit the data well, yielding χ^2 very close to unity (table 1 and 2). For brevity we do not consider mixed cases (BB + HA) in this paper because tests showed that in assessing absorption line significances (x4) they always produced results intermediate between the pure BB and pure HA cases. Continuum models with PL components are ruled out because they do not adequately fit the data, leaving significant residuals above 2 keV. Models I, II and III with thermal continuum components are all acceptable and cannot be distinguished statistically.

Figures 1 and 2 show the spectra and residuals for the best fit to model I (BB + BB) using the PN singles/doubles events and MOS1/MOS2 data respectively. The small residual at 0.7 keV was mentioned by DL04. However it does not statistically affect the global fits and we do not consider it further in this paper.

We show our best-fit continuum parameters and 90% confidence levels for six different models in the energy range from 0.3–4.0 keV for PN in Table 1. Each of these continuum models consist of two thermal components, either two blackbody or two hydrogen atmosphere models, and Gaussian line fits to the two broad absorption features. These models yield excellent fits to the data with χ^2 values for PN slightly less than unity. We found that Gaussian line profiles yield a statistically good fit to the data. The PN blackbody models I, II and III all give consistent values for these parameters.

We note that for some of our models the line depths (especially for the 1.4 keV line) are not well-constrained. This is caused by the presence of two continuum components. As described previously, the line can be on either of the continuum components or both. If the absorption feature is fixed to solely reside on one of the continuum components then the level of that component becomes very important. If the depth of the absorption feature is close

to the continuum level the residuals cannot be adequately fit rendering the line depth poorly constrained. This is evident in Table 1 for model I(BB+BB) where the 1.4 keV line is on the lower temperature blackbody. The continuum level of the lower temperature BB continuum component above 2 keV is negligible and the upper limit of the optical depth of a feature there is extremely poorly constrained. We note that it is possible for both of the broad absorption features to lie on the higher temperature continuum component (C1+C2-L1-L2). However, the fit was not acceptable leaving significant deviations from the data.

3.5. Comparison with the results of Bignami et al. (2003) and De Luca et al. (2004)

B03 also fit two continuum components plus two absorption lines to the XMM-Newton data. Their best fit continuum model consisted of two blackbody components. Later DL04 reanalyzed the same XMM-Newton data in the energy range from 0.3-4.0 keV with the SAS version 5.4.1. They also used two lines and two blackbody components. In both cases the best fits to the data yielded χ^2 significantly greater than one, leading B03 and DL04 to add two additional absorption lines to fit some higher energy residuals. They concluded that the fits to their data were substantially improved and that the additional lines were statistically significant.

We also fit two continuum components and two absorption features to the data but reach profoundly different conclusions. Here we focus on the dramatic differences in the statistical quality of the fits between B03/DL04 and us when only two lines and two continuum components are utilized. This is of critical importance because any statistical analysis of the need for additional line features will of necessity have as its starting point the quality of the statistical fit without those lines. We defer a careful discussion of statistics to x4.

Firstly we note that we considered a much broader set of continuum models than did DL04. They considered model III whereas we also considered models of the form I and II. We obtained excellent χ^2 for all these models. In the case of model III, our derived parameters are consistent with DL04 within the 90% confidence levels, and the very small deviations between us are likely due to their use of asymmetric line profiles. Hereafter we emphasize model III where our comparison with B03 and DL04 is direct, but our conclusions concerning the statistical superiority of our fits holds for all three classes of models.

In order to do a direct comparison of the quality of our fits with those of DL04 we used their published results to determine the χ^2 of their fits prior to adding a third and fourth line. We concentrate on DL04 because that work is meant to supersede that of B03. From table 2 of DL04 (where they list the χ^2 and degrees of freedom of their best fit three line model and the confidence level on the fit to the third spectral feature) we estimate their χ^2 before fitting a third spectral feature. For PN, MOS1 and MOS2 these numbers are $\chi^2 = 1.8, 1.3$ and 1.6 respectively.

These are clearly poor fits to what we call model III. It is evident from table 2 that our best-fit χ^2 are substantially less than those of DL04 for all three instruments. Moreover we obtain superior fits to the data for models I and

II as well. We do note that for the MOS data we found it preferable to fit the data in the 0.5-4.0 keV region, rather than the 0.3-4.0 keV region we used for the PN data and by B03 and DL04. The parameters derived for our fits are statistically in agreement with our PN results and the parameters derived by B03/DL04. Given that DL04 noted the observed time evolution of the redistribution function of the MOS detectors below 0.5 keV, this restriction of the MOS fits to greater than 0.5 keV seems prudent.

We are forced to conclude that DL04 simply did not find the global minimum in their binned spectra, but rather a local minimum. This led to poorer statistical fits and to increased significance of the third and fourth spectral features. We provide additional evidence for this interpretation later.

3.5.1. Investigation of effects of spectral binning

One possible source of the discrepancy between DL04/B03 and us could be differences in binning of the data. Our fit statistic should be χ^2 distributed provided we have enough counts per bin. We have more than enough (> 40 counts per bin) to satisfy the requirement for what is technically referred to as a "distribution free" statistic. For the MOS1 and MOS2 data we have about the same number of spectral bins as B03/DL04, yet we obtain significantly lower reduced χ^2 . For the PN data B03/DL04 have 100 spectral bins, significantly less than in our PN singles analysis (dof = 400). To see if this could explain the discrepancy, at least in the PN singles data, we rebinned the PN singles data by various factors using the ftools command "rbnpha". The spectra were then further binned by "gppha" such that each bin contained at least 40 counts.

χ^2 increases as the number of spectral bins decreases. This is expected as there is a tradeoff between having enough events per bin to satisfy the normality requirement for the

χ^2 distribution to correctly describe the asymptotic performance of the fit statistic versus the loss of information from that statistic encoding less of the spectral structure as the bin size is reduced. Nevertheless we note that our

χ^2 is still significantly lower than that of B03/DL04 when we used a comparable number of spectral bins and fit the data with model III.

We also fit the data with a third spectral line, calculated χ^2 , and evaluated the difference of χ^2 between the third line/no third line case. As we will see in x4, χ^2 is the key factor in determining whether a third line statistically improves the fit to the data when using a likelihood analysis. There is a small high energy residual as reflected in the fact that χ^2 is improved by the addition of a third line. We found that our χ^2 for both model III, using the same number of dof as B03/DL04, and for all our other models, did not change when we varied the number of dof over a range extending from our dof for the PN fits down to a dof significantly smaller than that which B03/DL04 used (table 3). This indicates that our analysis is robust to the number of spectral bin used and this χ^2 is significantly smaller than that of B03/DL04. This result serves as the basis for a likelihood analysis in x4.

We emphasize the important technical point that we selected our actual bin size, consistent with the requirements for a distribution free test, *a priori*, not by adjusting the bin size empirically in order to obtain the lowest χ^2 . It is

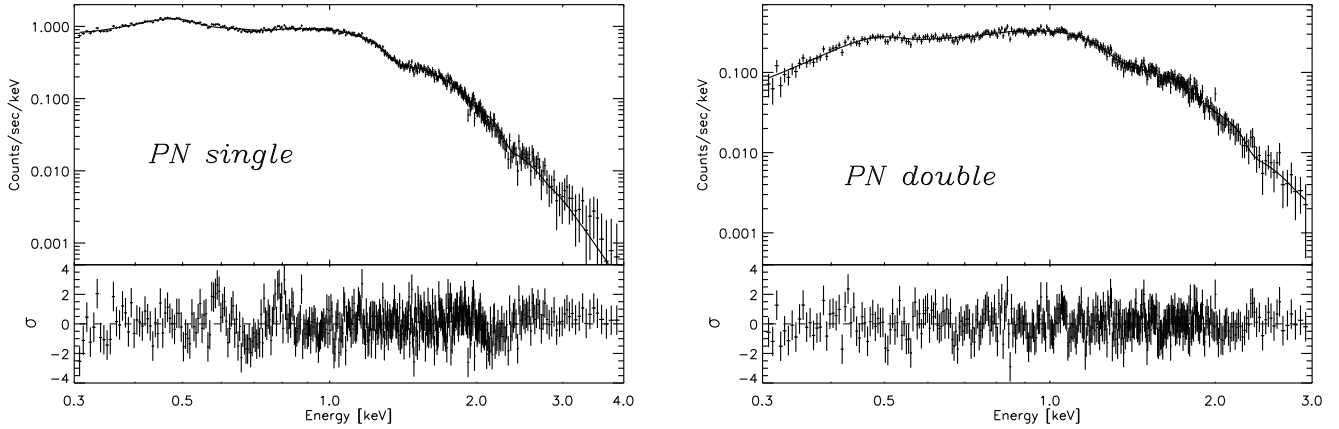


Fig. 1. | PN-single (top) and PN-double (bottom) spectra fit by $I(BB+BB)$ model and their residuals.

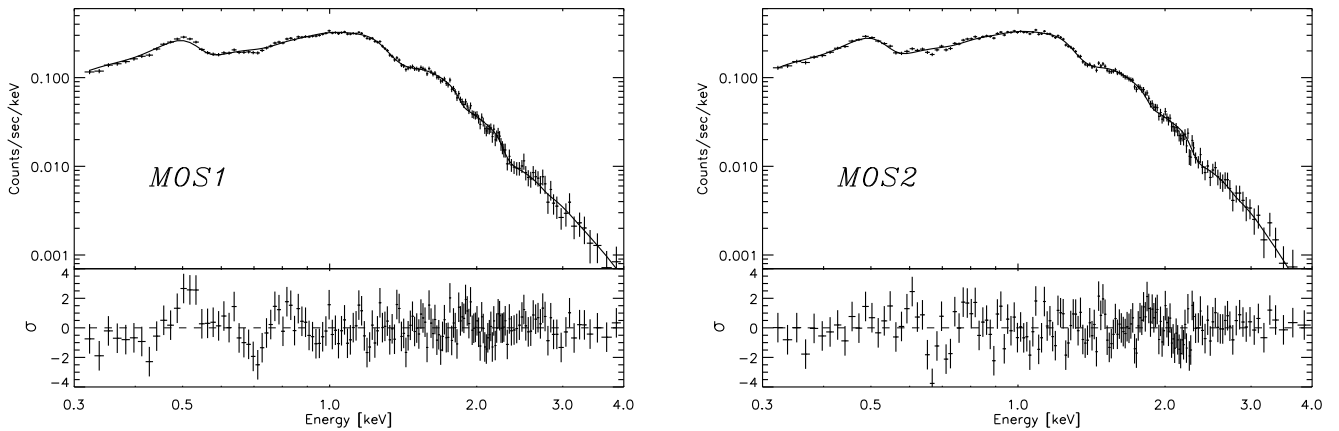


Fig. 2. | MOS1 (top) and MOS2 (bottom) spectra fit by $I(BB+BB)$ model and their residuals.

well known that in that case the resultant χ^2 statistic is not χ^2 distributed (Eadie et al. 1983) and would invalidate our direct comparison with the analysis of D L04/B 03.

4. statistical tests for extra spectral features

While it may naively appear that assessing the existence of and need for an extra spectral feature in a continuum spectrum is straightforward, this is not true. We present three approaches for assessing the need for extra spectral features. Our presentation brings together disparate results in the astrophysics and statistics literature. Given the importance to the underlying NS physics of establishing the existence of additional lines or the lack thereof in the 1E 1207 spectrum, our presentation is of necessity systematic and detailed. This is particularly true in the case of the F-test analysis of B 03/D L04; their analysis is incorrect for reasons well-established, if not well-known, in the statistics and astrophysics literature. Some time must be devoted to explaining this. We do note parenthetically that it is not for naught that the XSPEC users manual warns not to use the F-test for evaluating the need for additional line features in a spectrum, although they do not explain why. We present the explanation in x4.1, where we discuss likelihood tests and their close cousin F-tests. In

x4.2 and x4.3 we consider two other methods for attacking this problem.

4.1. Likelihood ratio test and F-test for detecting extra model components

The general principles of application of the likelihood ratio test (LRT) and F-test are well-known to most astrophysicists. We review the formalism here since it will provide a context for explaining when the tests as commonly employed are valid. Also we intend to apply these tests in x4.1.4, so understanding this formalism is important. The following few sections follow and summarize the arguments of Protassov et al. (2002) (hereafter P 02). The reader is referred to this paper for a very lucid and more extensive discussion than we can give. We have kept close to the notation of P 02. As in P 02 we use the likelihood test as the basis of our discussion for clarity, but as they point out, identical considerations apply in an obvious fashion to the F-test and χ^2 tests, which we employ.

4.1.1. General considerations

The models we posited in x3.3, when propagated through a suitable response matrix of the instrument, provides a prediction for the number of counts in bin i , say

x_i . The counts in bin i further depend on a set of parameters say $\theta = (\theta_1, \dots, \theta_p)$. These include the spectral indices and normalization of the continuum and the line parameters (optical depth, width, line position etc.). The counts in bin i are Poisson variables, or if the counts are large enough, Gaussian-normal variables. The primary goal is to determine if θ , which reflects the presence of an absorption line, is non-zero in a statistically meaningful way, and secondarily what the parameters of the line are. This can be done through the application of the familiar likelihood ratio test or the F-test. In the case of the LRT with measured counts in bin i we have

$$R = \frac{\max_{\theta} \int_{x_{ij}}^{x_{ij+1}} f(x; \theta_0, \dots, \theta_{q+1}, \dots, \theta_p)}{\max_{\theta} \int_{x_{ij}}^{x_{ij+1}} f(x; \theta_0, \dots, \theta_q, \dots, \theta_p)} \quad (2)$$

where the $\theta_0, \dots, \theta_q$ are values held at their true values under the null hypothesis (no line) and $\theta_{q+1}, \dots, \theta_p$ are parameters free to assume any value that maximizes $f(x; \theta)$, the probability distribution function. The denominator is the same function only now all parameters are allowed to vary. Symbolically we can write this as

$$R = \frac{\max_{\theta} L_{\text{unconstrained}}(x_j)}{\max_{\theta} L_{\text{constrained}}(x_j)} \quad (3)$$

where constrained refers to the fact that some parameters are held at their assumed value under a null hypothesis, H_0 , and the L 's are the likelihoods. In the case of 1E 1207 the constrained parameter is θ_0 . Fundamental theorems of statistics then establish that under the null hypothesis $2 \log R = T$, the likelihood ratio, is asymptotically distributed like χ^2 with degrees of freedom (dof) equal to the number of constrained parameters.

Very heuristically T is seen to be just the difference of the constrained and unconstrained χ^2 , for the case of normal errors in f , the distribution function. The test statistic F is constructed from this difference divided by the χ^2 , so it is also similar to a likelihood test (see P 02 for details).

4.1.2. Conditions for Validity of LRT and F-test

The LRT and F-test are extremely powerful because they are "distribution free." That is, in the asymptotic (large count) limit, and under the null hypothesis, they do not depend on the initial probability distribution function in L at all. They only depend on the "reference distributions" of χ^2 and F . This asymptotic behavior effectively decouples details such as shape of the continuum and the particulars of the line profile and strength from the way the test statistic is distributed asymptotically. This is why the tests are so powerful and so broadly applicable.

However for the LRT and F-test to be distribution free asymptotically there are certain regularity and topological conditions that must be met. The regularity conditions are requirements on the derivatives of the probability distribution function f with respect to parameters, as well as certain probability measures (integrals) of f and its derivatives. These can be found in textbooks (Serfling 1980; Roe 1992). They are of no interest to us since they are weak conditions almost always satisfied in astrophysics modeling. Of profound importance though are the topological conditions (P 02). These are: 1) the model under test must

be nested, that is, the parameter under test in the constrained model must be a subset of that parameter in the unconstrained model and 2) the parameter under test in the constrained model cannot lie on the boundary of the possible values of the parameter under the unconstrained test.

Evaluating these topological conditions for equation (1) we see that the first is met; the constrained model has $\theta_0 = 0$ and thus the parameterization in the constrained model is a subset of that in the unconstrained one. However condition 2 is violated. $\theta_0 = 0$ is on the boundary of the possible values θ_0 can assume under the unconstrained model.

4.1.3. Invalidity of B 03/D L04 statistical analysis

The simple observation that topological condition 2 is violated completely invalidates the F-test analysis of B 03/D L04. The test statistic F which they used does not even asymptotically approach the F -distribution. One cannot make any statement about the presence of a line, or its significance, based on their analyses. P 02 illustrate this through a variety of simulations for the case of both emission and absorption lines added to a continuum source. In their emission line simulations the expected reference distribution underestimates the strength of lines significantly (compared to the actual distribution that should be used) and in the case of absorption lines overestimates the strength of lines by almost an order of magnitude. As P 02 properly notes, in general nothing can be said about the significance of a line, since we do not even in principle know the asymptotic reference distribution.⁴

We have shown in x3.5 that B 03/D L04 did not find the global minimum of the model without additional absorption lines. This, we shall see in a more careful analysis below, leads to an evaporation of the statistical significance of their lines. But more importantly, even if their continuum fits were correct, their statistical analyses would still be wrong. As we show below, and consistent with the conclusions of P 02 for absorption lines, the standard F-test grossly overestimates the necessity of the extra line. The B 03/D L04 analysis can produce no meaningful result because they have no valid reference distribution.

4.1.4. Analysis of 1E 1207 line significance using modified LRT and F-test

In x4.2 and x4.3 we give less complicated methods for assessing the presence of a line in the 1E 1207 data. However we thought it instructive to simply follow the straightforward, if somewhat laborious, approach of P 02 for "fixing" the problem noted above. We employ the F-statistic, which we now understand is not "F-distributed." What is now required is the establishment of a reference distribution for line statistics, since it is clear an appropriate asymptotic distribution does not exist, even in principle. This does not prevent one from finding an appropriate reference distribution but it will of necessity depend on the details of the model e.g. the continuum fit, the line parameters and profile etc.. We can find the reference distribution via computer simulation. We might naively assume that we could accomplish this task by fixing all

⁴ This is a good place to note that the editors of *Astrophysical Journal* chose to subtitle the Protassov et al. (2002) paper "Fallible F-test" on alternating pageheads.

model parameters, except those associated with the line, at their best t values under the null hypothesis. And then we would repeatedly generate fake data from which we could determine the relevant reference distribution. This is in fact the technique of bootstrapping. However this is not correct since we do not know the "true" values of the parameters to use in the simulation. The failure of the topological condition 2 means that we lose conditioning properties that would make it meaningful to replace the parameters by best estimators which can serve as the ersatz "true" values.

A solution to this problem (as pointed out in P02) is to use parameter values in the simulation that are likely given the observed data. This simply requires a statistical distribution of parameter values which can be sampled and incorporated into the simulation which generates the distribution of the statistic. P02 advocates a Bayesian approach for determining the probability distribution of each parameter, given the data. The Bayesian formalism gives the probability distribution of a parameter given the data x and prior information I in terms of a model for the data x , given I , and a distribution reflecting our previous knowledge about I .

$$P(\mathbf{x}; I) = \frac{P(\mathbf{x}; I)P(\mathbf{x})}{P(\mathbf{x})}: \quad (4)$$

The literature on Bayesian analysis, even in the specific case of astrophysics, is too enormous to cite. Moreover there are a variety of methods for most efficiently determining $P(\mathbf{x}; I)$ given varying degrees of prior information.

We have implemented the posterior predictive p-value methodology of P02, which uses this Bayesian information on $P(\mathbf{x}; I)$ to generate the fake data (from the real data) necessary to evaluate the distribution of a test statistic under the null hypothesis. This approach, while perhaps not previously familiar to the reader, is readily seen as nothing more than a way to implement a fancier version of the statistical bootstrap where the errors on the

fitting parameters are taken into account. This is clearly straightforward to implement in a Monte-Carlo by brute force although clever and efficient non-brute force methods for implementing the Monte-Carlo exist (van Dyk et al. 2001).

P02 pointed out that the general considerations above are valid for the LRT, the F-test and the χ^2 test (where we form the statistic $T = \chi^2_c(x; \cdot) - \chi^2_u(x; \cdot)$). We implemented the χ^2 test, as well as the F-test, but the results are basically identical. We only present the F-test results here to provide a direct comparison with B03/DL04.

4.1.5. Details of the line search procedure

The implementation of the procedure described above is straightforward although time consuming. We briefly discuss some technical details concerning the line search procedure. We simulated our spectra with parameters determined by Bayes formula. These spectra are folded through the instrumental response using XSPEC. The actual line search was done by performing a blind search for absorption lines between 0.3 and 4.0 keV. The statistic F was calculated as, $F = (\frac{\chi^2_c}{\chi^2_u})^2 = \chi^2$ (Bevington (1969); P02) where F is obtained from the fit to a continuum model (C) and continuum model plus absorption line

(U). A blind search for spectral features in fake spectra in XSPEC is dependent on the initial values and paths (Rutledge et al. 2002). In order to reduce this effect we started the line search from four different line energies. We may not find all the significant absorption lines when more than four are present in the simulated spectrum. However such cases, which entail a large F statistic, occur very rarely. To confirm this we performed Monte-Carlo simulations with an increased number of initial starting energies, and found that the number of occurrences of F larger than 5 did not change. In searching for a line from four starting locations we found that sometimes XSPEC fit the same feature more than once. We corrected for such double-counted events a posteriori.

The distribution of the statistic $F = \chi^2_c / \chi^2_u$ is shown in Figure 3. This distribution was determined for each instrument, although it did not vary significantly for the three instruments. In formulating this distribution we recall x4.1.1 that this corresponds to the distribution of F under the null hypothesis, i.e., that there is no line. This is what is shown in Figure 3, along with the classical F -distribution. We conclude that there are no grounds for rejecting the null hypothesis (no third line). The results are always in the 1-3 range and only reach the higher level in a few isolated instances involving black-body models and PN singles data.

Our results differ radically from B03/DL04 for two reasons. Firstly our F -statistic is about 50% smaller due to our better fits to the continuum. And secondly the use of the correct finite distribution for the F -statistic drops the significance of an extra absorption line by a huge amount, as happened in the likelihood simulations of P02. The net result is a more than six order of magnitude reduction in the significance of their strongest line, found in the PN data.

Further support for our conclusions is presented below, where essentially the same result is arrived at by different statistical tests.

4.2. Goodness-of-fit test for lines in smooth spectra

This type of test is described in numerous papers in the literature, but we will mainly follow the arguments and notation of Eadie et al. (1983). We will test the null hypothesis (H_0) that there is no deviation of counts with respect to the continuum level against the alternative (H_1) that there is such a deviation. We will define a test statistic T , and unless T exceeds some critical value T_c then we will accept H_0 . Under H_0 , T has some distribution $P(T \leq T_c)$. T_c can then be implicitly defined by the formula $= \int_{T_c}^{\infty} P(T) dT$ where P is defined by the 4-tail of a normal, standard distribution. This procedure ensures that the null hypothesis will not be rejected unless a 4 burden of proof is met. This test is binary - unless T exceeds T_c we accept H_0 . This result can be further quantified by calculating $1 - C = \int_{T_c}^{\infty} P(T) dT$. $1 - C$ can be converted into units of using the same method as employed for and provides a measure of how far our test statistic T is from the 4 result. C is the confidence with which we can reject H_0 .

We need only define our test statistic T and its probability distribution under H_0 . We are searching for a deficit of

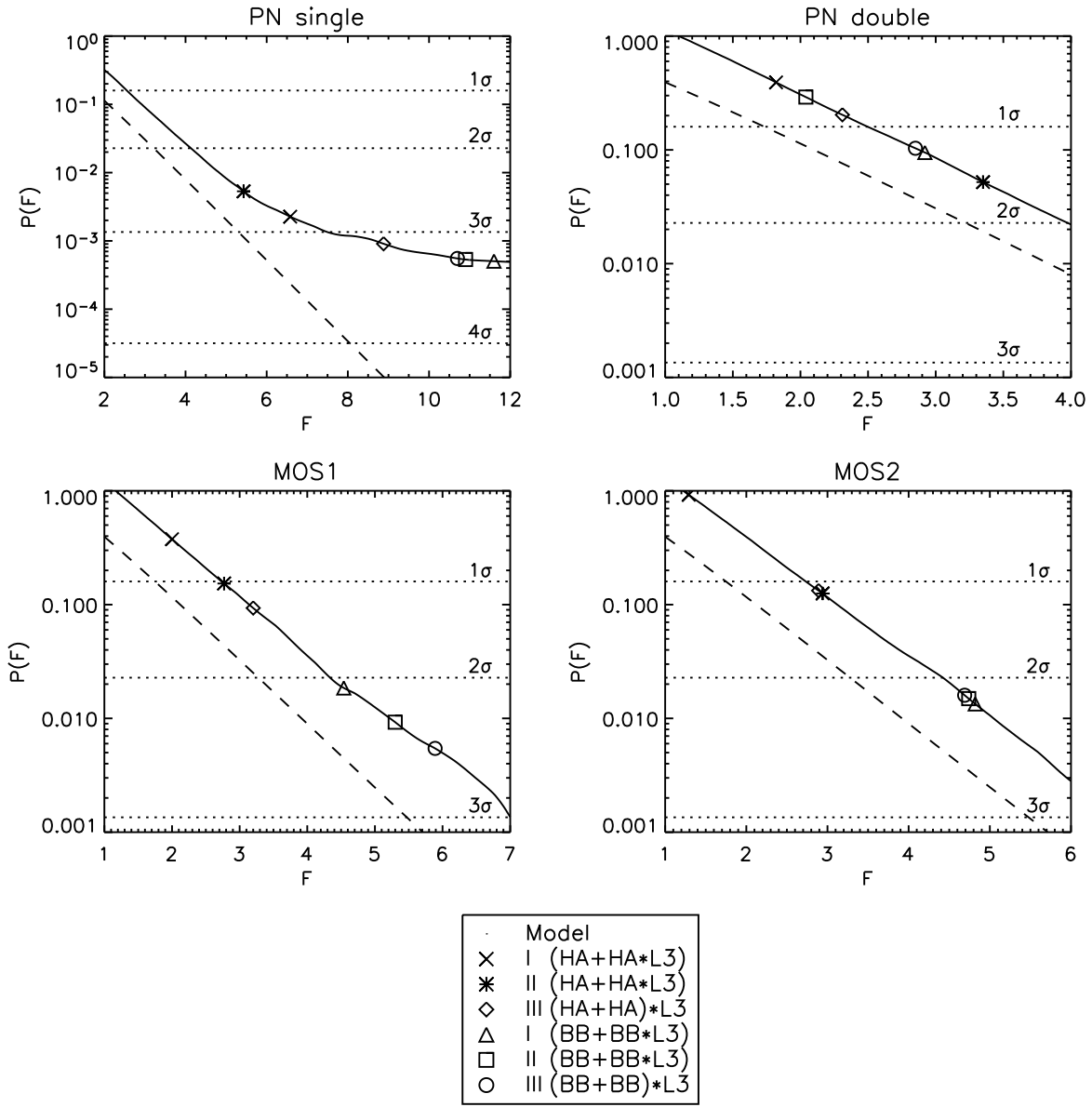


Fig. 3. | $P(F)$ distribution for four instruments.

counts in a region of the spectrum beyond that predicted by our continuum model. We will assume that the region of interest is defined by K energy bins around 2.1 keV. Define n_i = observed counts in bin i ; $s_i = n_i - \hat{b}_i$, b_i = true continuum in bin i and \hat{b}_i = estimated continuum in bin i . We can then formally construct the null hypothesis H_0 , there is no line, ($s_i = 0$ for all K) against all alternatives defined by H_1 . This is the classic goodness-of-fit test. The natural test statistic is $T = \sum_{i=1}^K \frac{(n_i - \hat{b}_i)^2}{\text{var}(n_i - \hat{b}_i)}$.

This can be expressed, under suitable conditions (appendix) as

$$T = \sum_{i=1}^K \frac{(n_i - \hat{b}_i)^2}{\hat{b}_i + \hat{\sigma}_i^2} : \quad (5)$$

This test statistic is composed of random variables $z_i = \frac{n_i - \hat{b}_i}{\sqrt{\hat{b}_i + \hat{\sigma}_i^2}}$ or equivalently $T = \sum_{i=1}^K z_i^2$. We restrict

this sum to the K bins of interest. Under the null hypothesis H_0 one can show (appendix) that for n_i not too small that the z_i are normal (Gaussian) and standard (mean 0 and variance 1). Thus under H_0 , T is by construction distributed with K dof. If $K > 30$ one can additionally show (appendix) that a new variable can be constructed $y = \sqrt{T/K} = \sqrt{2K}$ and y is asymptotically standard, normal. We select a T_c (y_c), and if $T < T_c$ ($y < y_c$) we accept H_0 (there are no counts in deficit of the continuum model). T_c is related to y_c as discussed above. y_c is similarly defined only with the standard, normal distribution replacing $P(T)$.

4.2.1. Results applied to 1E1207 data

For all the models we considered the observed T was much less than T_c so we accept H_0 - ie., there is no line. Table 4 lists the observed T and T_c for various models.

Note T_c changes for each model because of its dependence on the continuum level and the variances within that model. Table 4 also indicates $1/\sqrt{C}$, to give some feel for the "distance" of T from T_c in probability space. Because K is sufficiently large in this analysis, we formed the random variable y from the observed T , as mentioned above. This is shown in table 5 and provides a direct comparison of how close (far) the measured y is from y_c and the "center" of the distribution $P(y)$ in units of σ .

The formulation above is correct in searching a region where there is a priori reason to expect a line. There is a complication in how exactly to determine the K bins of interest (other than that they are around 2.1 keV). If the spectral feature is narrow and the region of the K bins broad, then the feature can be washed out. This is also true in the converse case. To be conservative we checked varying sized regions of interest around 2.1 keV. The results were not significantly changed for regions comparable to a few times the energy resolution (from less than to slightly greater than the widths reported in B03/DL04).

In such a blind search one must correct for the fact that there are N possible regions of interest (N is the energy band divided by the width of a single region of interest) in which to find a statistical fluctuation of a given level. Very roughly this increases $1/\sqrt{C}$ by the same factor, which is

6. A more detailed treatment can determine the exact factor (Eadie et al. 1983). We have neither corrected for this factor in this section nor reduced the significances in the next section accordingly. Our results should be considered in upper limits in this regard.

4.3. Significance of the absorption lines by equivalent width

The natural and perhaps most straightforward method for deducing an absorption feature's existence is to simply assume it exists and estimate the significance of the detection. In this section we evaluate the significance of the residuals around 2.1 keV by fitting a Gaussian absorption profile, and then calculate the equivalent width (EW) and error bars. This particular absorption line profile gives excellent fits to the data ($\chi^2/1$), so no improvement would be had by alternate line shapes. We considered other line shapes did not statistically significantly affect either the EW or the line position. Of critical importance here is a proper calculation of the error on the line fit. This is a standard non-linear χ^2 fitting problem of the type discussed by Lampton et al. (1976) (LM B). We follow their approach exactly. The spectrum is fit allowing all the continuum parameters to vary freely, and the line depth and width are stepped through. The minimum value of χ^2 is jointly estimated for the line depth and width. A contour plot of the 68% confidence interval for line depth and width is then calculated using the prescription of LM B. Using the 68% ($\pm w$) contour we integrate to find the EW extrema, and the best fit ($\pm w$) provide the best estimator of EW. We held the line centroid at its best-fit value during this procedure to save computational time. A series of test runs indicated that the EW depended only weakly on line centroid within the 68% confidence interval. The contour plots (68% confidence) are shown for the PN single and M0S1/M0S2 data in figure 4, for model III(BB+BB)*L3. In the case of the M0S data the errors

in depth and width are highly correlated, highlighting the importance of a joint estimation of the errors using the procedure of LM B.

The results of this analysis are shown in table 5 for all the relevant models. In no case is the statistical significance of the line detection larger than 2. The strongest residuals are for PN data, and the EW for these cases are shown in figure 5. Except for the black-body models, the M0S1/2 residuals were essentially non-existent, so we gave up attempting to fit them. In some cases in table 5 the absorption line resided on a low temperature black-body component which was so weak that no EW could be determined. We note for thoroughness (although we think it obvious) that one must calculate the EW using both the low and the high energy continuum components, even though the physical model may indicate the line only resides on one continuum component. Calculating the EW in this latter case may be physically important in interpreting the physics, but in assessing the existence of a line only the former procedure has statistical significance.

4.4. Concluding remarks on line search

We have used three different methods to demonstrate there is no spectral line in the 2.1 keV region. A summary is presented in table 5. The level of significance of the third spectral feature and measures of its significance are consistent with each other. In only a few isolated cases of black-body continua does the line rise even to the 3 level, much less something really indicative of a line. Since the fourth spectral feature is much, much weaker than the third feature, we gave up analyzing it in detail. In x6 below we will present plausibility arguments that the statistically insignificant spectral residual in the PN data is due to instrumental effects.

5. Phase-resolved spectral analysis

While no evidence of a third spectral feature was found in the time-averaged data for thoroughness we decided to repeat our analyses for phase-resolved data. First we searched for the spin-period using the PN data after correcting photon arrival times to the barycenter. PN was operated in small window mode with time resolution 6 ms. The M0S data does not have sufficient time resolution for spin-period determination. We used XRONOS 5.20 for our timing analysis. Using the Epoch-folding method we found significant pulsation at $P = 424.13076 \pm 0.00002$ sec, consistent with the results of B03 and DL04. After tagging photons with the best-fit spin-period, we reduced spectra in four spin phases following B03 and DL04. Spectral bins were binned to have at least 40 counts in each bin. Figure 6 shows phase-resolved spectra fitted with continuum model I(BB+BB) and residuals. We fixed N_H to the fitted value (1.32×10^{20} cm $^{-2}$ from the phase-averaged PN spectral analysis). Our results did not change when we let N_H vary in spectral fitting.

At around 2.1 keV, only a few spectral bins deviate from the continuum model, and residuals are comparable to or smaller than the energy resolution, indicating that they are due to statistical fluctuation. This is borne out by statistical analysis of the residuals using the approach of x4.1. Figure 7 summarizes the results for the statistical tests on the phase-resolved data. There are no spectral features.

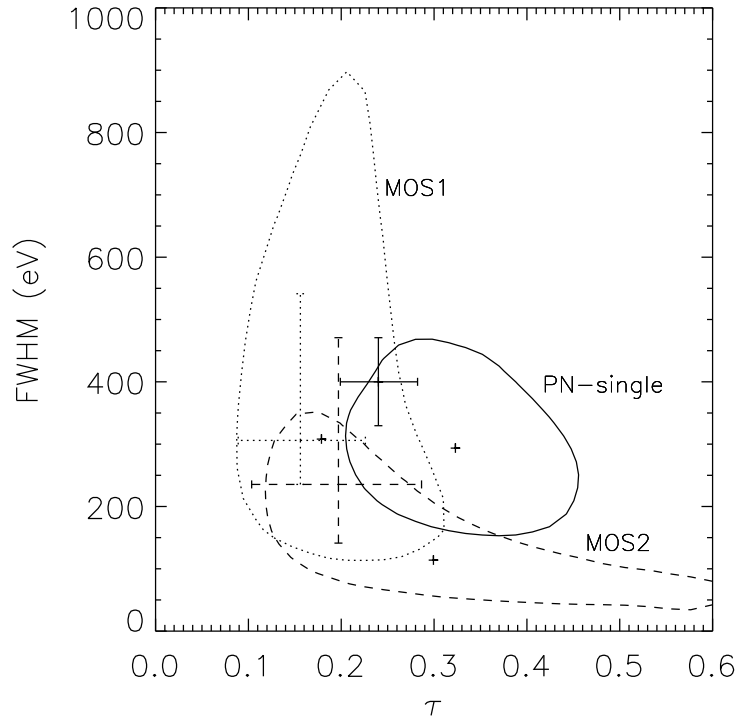


Fig. 4. χ^2 contour plot for a 3rd line (PN, MOS1 and MOS2). The contours were calculated at 68% confidence level. We fit model III(BB+BB)*L3 to the data. The crosses show the best-fit parameters at 90% confidence of DL04 (Solid = PN, dashed = MOS1, dotted = MOS2).

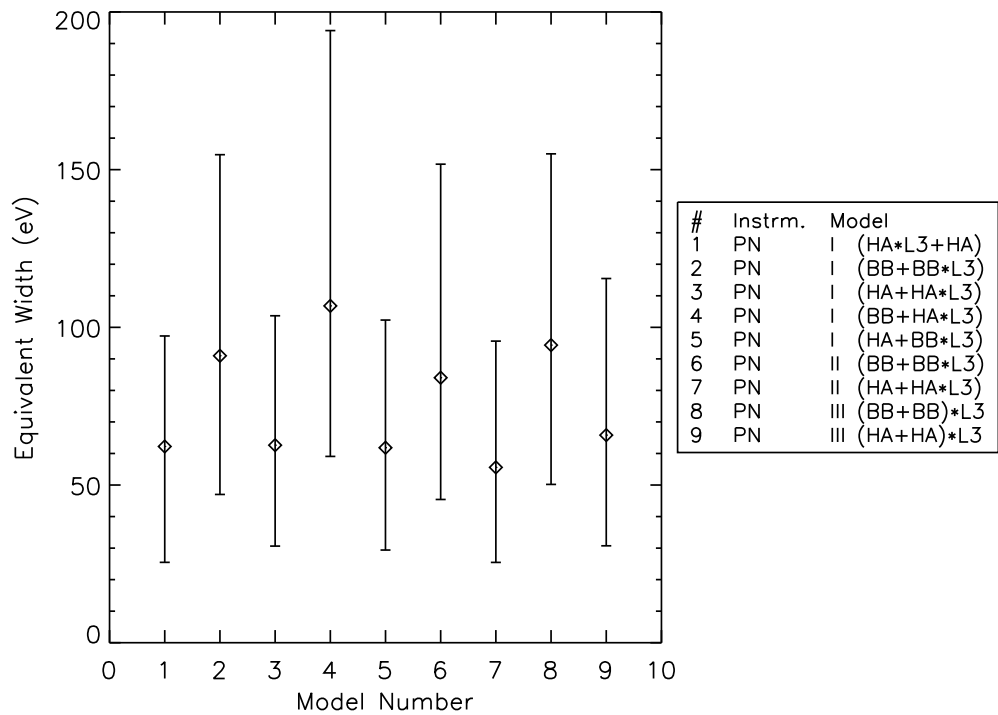


Fig. 5. Equivalent width [eV] of a 3rd line at 2.1 keV and 68% confidence levels.

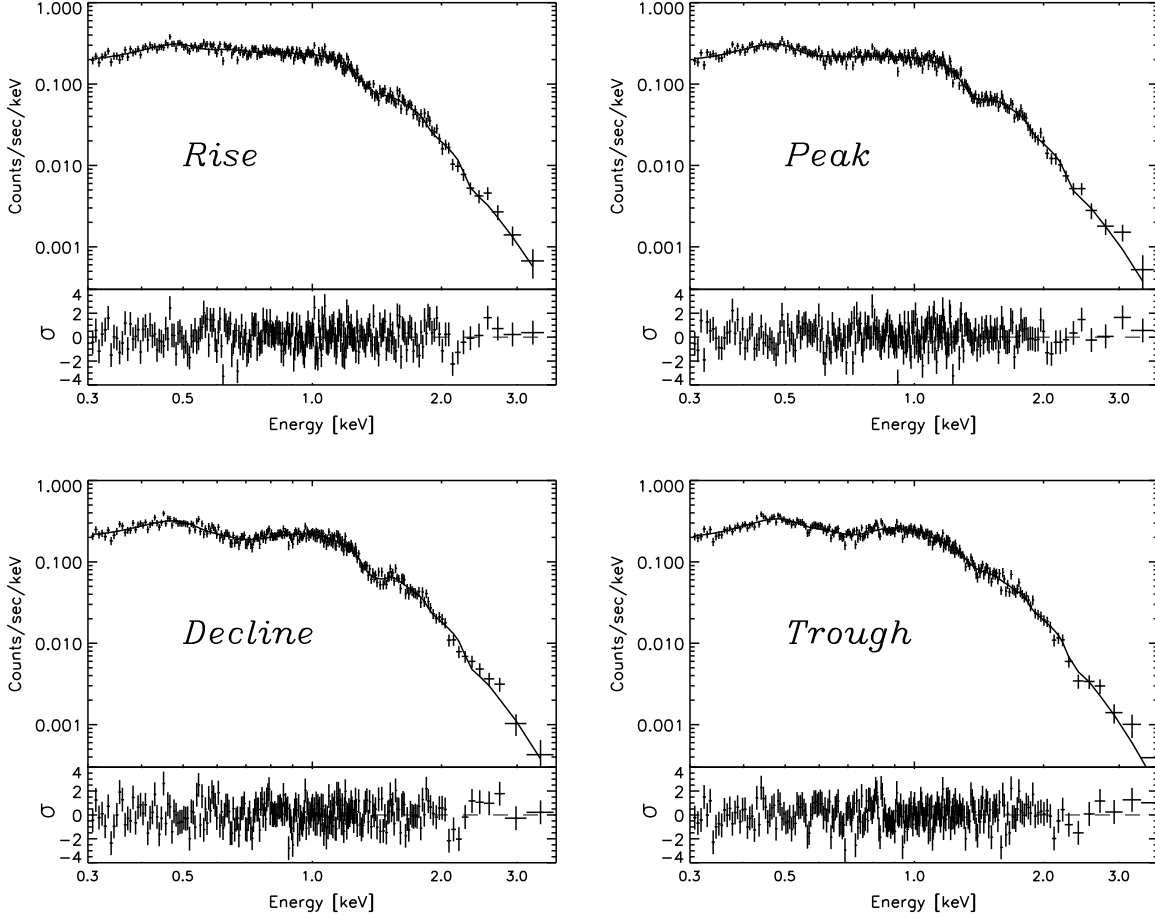


Fig. 6. Four phase-resolved spectra and residuals fit by model I (BB + BB).

6. physical significance of the residuals in the continuum spectrum

We have demonstrated that there is no third line in the 1E 1207 spectrum. Thus any attempt to explain the origin of 1{3 residuals should be considered suspect. We have several ground rules in this section. We explicitly avoid detailed fitting of line shapes and in-depth searches for specific instrumental origins of the residual. It would certainly be futile given the strength of the residuals, and we are unlikely to offer deep insights into possibly subtle instrumental effects. Finally we concentrate on motivating our suspicions using PN data, since the residuals are marginally stronger and thus likely to be more fruitful hunting ground.

6.1. Analysis of residual line centroids

The analysis of x4.3 yields the centroid of the weak residuals for each of the models described in x3. A plausible hypothesis is that the residuals are associated with the Au{M edge, which occurs in the PN and MOS instruments. B03/DL04 worried about this possibility, but dismissed it. To pursue this hypothesis we need to focus particular attention on the line centroids associated with model III. If the residuals arise in the Au{M 5 edge of the instrument, then model III clearly corresponds to the only physically correct model for the data. So if this hypothesis is true,

we expect to see residuals around the Au{M 5 energy.

Figure 8 shows the line centroids from ts to the third line using model III for PN single data, PN double data and combined PN single and double data. We also show the B03/DL04 90% confidence interval band for their line centroid determination. The dotted line is the theoretical position of the Au{M 5 edge. The striking feature of this plot is that the PN single data, which is without question the most reliable data since it rejects split events, occurs at the position of the Au{M 5 edge. Moreover the potential origin of the lower residual energy for B03/DL04 is suggested by the fact that the PN doubles (split events) occur at lower energy and that our combined PN data set is more in agreement with the results of B03/DL04. The PN split events have reduced the energy of the residuals, while the pristine PN singles events are at the expected energy for an instrumental effect. One would be tempted to say this lower energy in the split events is expected. This would get into a discussion about how well split events are reconstructed in EPIC data and is far too detailed for us. We simply note that the highest quality event data shows residuals at the Au{M 5 edge and the lowest quality data shows it at much lower energy. We also show in figure 8 the position of the residuals in 3C 273, using a fitting procedure described in the next section. The 3C 273 residuals, which are most certainly associated with the Au{M 5 edge, define the "t" position of the Au{M 5 edge and is a more

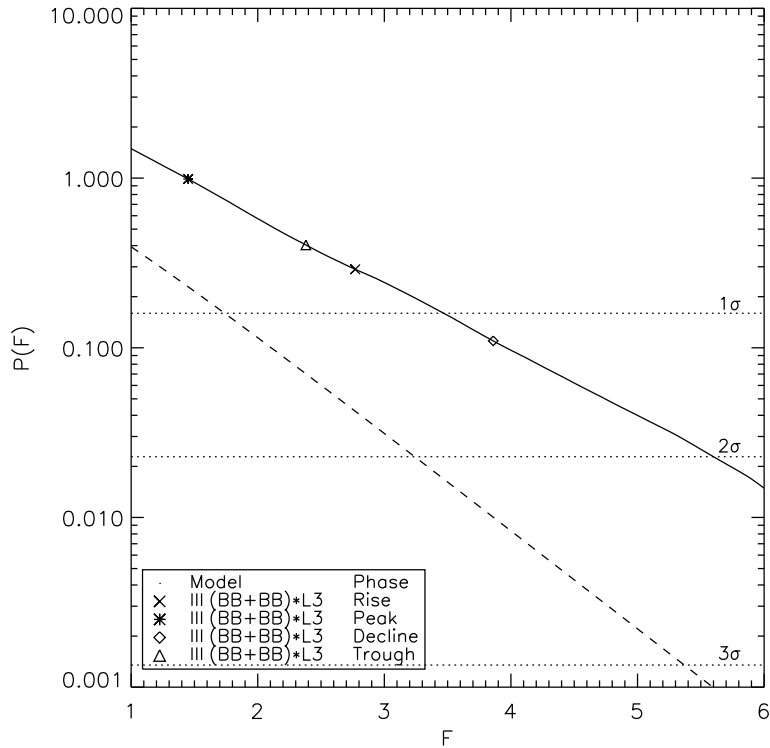


Fig. 7. | $P(F)$ distribution for phase-resolved spectra.

relevant metric than the theoretical position of the edge. Nevertheless, the position of the AuM feature in 3C 273 is consistent at the 90% level with the theoretical AuM energy and it is also consistent with the position of the residuals in the PN singles data. A better line shape approximation would no doubt move the 3C 273 result downwards, but this would require detailed understanding of the instrument response. Our results are meant only to be suggestive since, after all, the residuals are statistically insignificant, so we must be cautious at reading too much into them. But this analysis is highly suggestive of an instrumental origin for the weak residual.

6.2. Consistency test between PN and MOS data

One puzzle in the results of DL04 is the some six orders of magnitude difference in the statistical significance of their line detection between PN and MOS instruments. This inconsistency occurs despite the fact that their PN and MOS continuum parameters are in good statistical agreement. B03/DL04 attributed this to calibration uncertainty of the MOS detectors at low energy, even though they specifically avoided fitting the continuum in MOS at the lowest energies precisely to avoid calibration problems. In contrast, in this section we explicitly demonstrate that our PN and MOS analyses of the line are statistically consistent with each other. Thus low energy calibration uncertainties, at least in our analysis, are not a problem.

We set up a Monte-Carlo simulation to test whether the 3rd line residual detected by PN could have appeared in MOS data as a deficit with a significance comparable to that observed. We used the $III(BB+BB)*L3$ model fit to the data because this is the model DL04 used and it

showed the largest significance of a 3rd feature, therefore the largest discrepancy between PN and MOS. Hereafter we describe our formalism using PN-single and MOS1 case as an example: (1) we fit the model $III(BB+BB)*L3$ to the PN-single data and calculate best-fit parameters (2) we fold the model with variance in both the continuum and line parameters through MOS1 detector response and simulate a spectrum with the same exposure time and spectral bins as our analysis of the real data. (3) we evaluate χ^2 by fitting a fake spectrum with and without a 3rd line. We repeat this procedure 1000 times and compute the distribution of χ^2 . Figure 9 shows the results from the consistency test between PN and MOS1 (left) and PN and MOS2 (right).

We calculated the fraction of simulated χ^2 points smaller than or equal to the measured $\chi^2(S)$, i.e. $f(\chi^2 \leq S)$. The results are $f(\chi^2 \leq S) = 1.7 \cdot 10^{-3}$ (MOS1) and $f(\chi^2 \leq S) = 4.1 \cdot 10^{-3}$ (MOS2). The PN and MOS1 results are just consistent at the 2.93 level and at the 2.64 level between PN and MOS2. We conclude that the behavior of PN and MOS instruments is internally consistent with regards to fitting of the lines, as we showed previously was the case for the continuum fits.

6.3. Strength of the residuals in the AuM region

Although they cited a centroid position discrepant with the AuM complex at the 90% confidence level, B03/DL04 were still worried enough to explore the possibility that they were simply observing the AuM complex. We also decided to pursue this analysis, using XMM-Newton data on the quasar 3C 273. Residuals from the AuM complex show up strongly in the continuum spectrum of 3C 273.

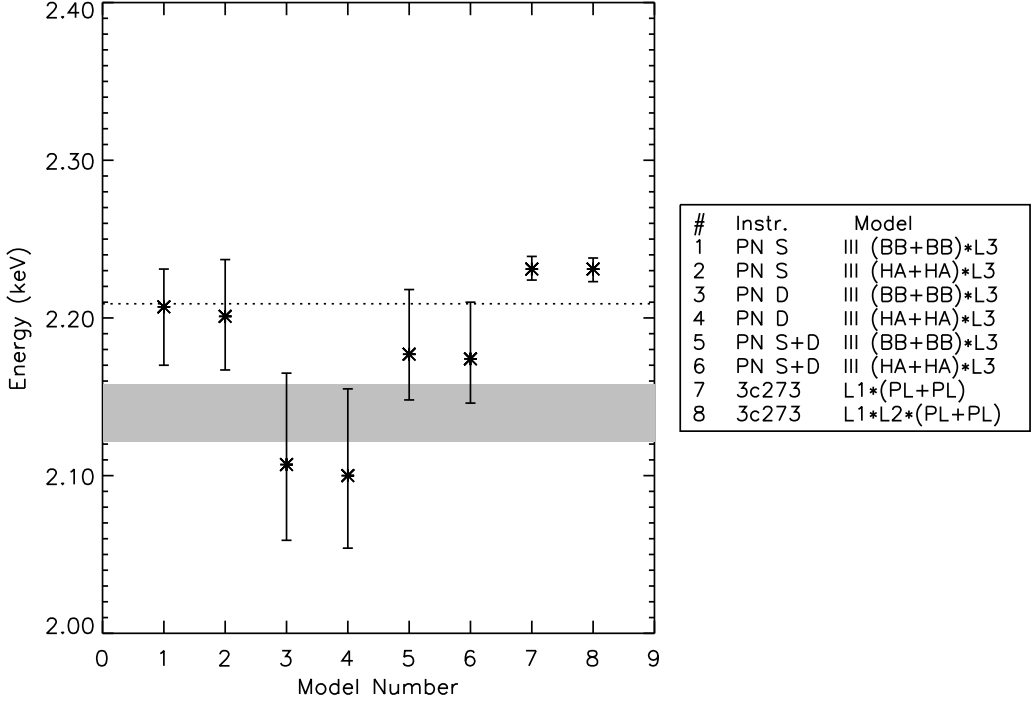


Fig. 8.1 Line energy of a fitted 3rd line. The shaded region indicates the 90% confidence level found by DL04. All error bars are 68% confidence. The dotted line is at AuM 5 edge position.

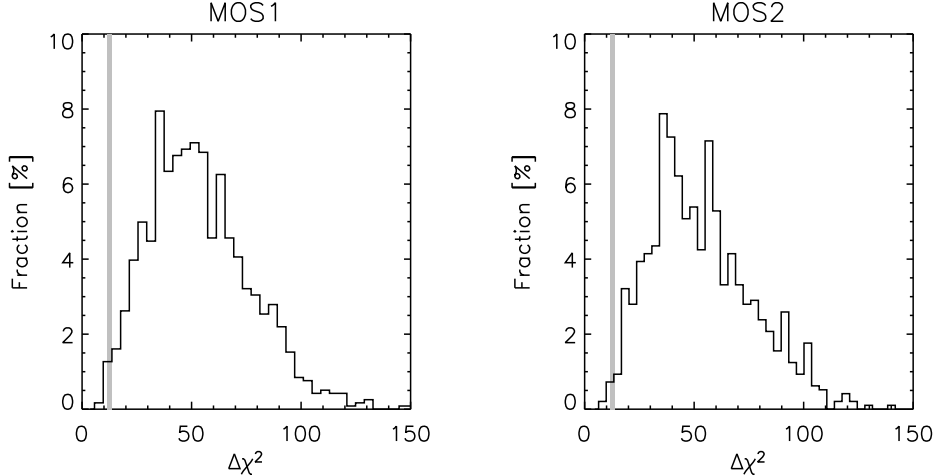


Fig. 9.1 Results from the consistency test for PN-single data. The grey lines correspond to the measured $\Delta\chi^2$ values in MOS1 and MOS2 data.

A comparison of the EW of the residuals in 3C 273 and 1E 1207 can shed light on whether the feature in the latter's spectrum is real or not.

We extracted PATTERN 04 events from a 40" radius region centered on the source. We used a double power law continuum model to fit the PN singles data in the 0.3–6.0 keV energy range. We did not bother to fit the AuM region but instead fit our model III with blackbody spectra for 1E 1207 and double power-law continuum for 3C 273, and plot the ratio of the residuals to the model spectrum. We note that the residuals are 6.7% in the quasar data

and 10.15% in the neutron star data. The neutron star data has larger error bars.

As a sanity check on our analysis we directly calculated the EW of the 3C 273 residuals at 2.2 keV from the data and obtained 8 eV. This is in agreement with both DL04 and the XMM-Newton calibration team. Calculating the EW for 1E 1207 directly without resorting to a line fit gives 40 eV. This is consistent with our EW determined by line fitting and is only 5 times larger than the EW in 3C 273 rather than the 13 times larger effect claimed in DL04 for the ratio of EW for the quasar and neutron star. Of course

this ratio is somewhat irrelevant. The EW for 1E 1207 is larger than that for 3C 273, but not statistically significant. Moreover figure 10 (left) shows, the noise level in the neutron star data is much higher, and there are comparable sized fluctuations elsewhere in the spectrum.

A more dramatic way to see that there is no strong residual is to plot the difference between the continuum model and the actual data in "error" space. In figure 10 (right) we show the residuals between the continuum model and the data in units of the 1 error bar on the residuals. The same plot is shown for 3C 273. We see that there is nothing extraordinary in the neutron star data. The fluctuations are uniform through the entire spectrum because the residuals are so weak. In 3C 273 the Au-M edge is readily apparent because of the better counting statistics.

As a final note we comment that it is easy to understand why B03/D L04 concluded that the residuals in the neutron star spectrum were markedly stronger than in the quasar spectrum. They fit the neutron star spectrum with four absorption lines and a continuum, and then used the resultant continuum as a basis for comparison with the residuals. This procedure is incorrect since it grossly overestimates the continuum, and thus the strength of the dips with respect to it. The correct procedure is to compare the dips with respect to the best fit continuum. This markedly reduces the significance of the residual, in complete consistency with the results we presented in x4.

7. conclusions

We have shown that the F-test analysis used by B03/D L04 is flawed. It violates topological conditions required for the test to have a well-defined asymptotic statistical reference distribution (the F-distribution). Calculating the correct, finite statistics reference distribution for the F-statistic, we find the third and fourth line are statistically insignificant. This is consistent with previous simulations done on absorption lines by P02.

We have shown that B03/D L04 only found a local minimum in χ^2 in fitting the continuum. With careful fitting we find χ^2 much lower than they did

for the continuum fits, and we find such low χ^2 can be obtained for a much wider range of physically acceptable models than B03/D L04 tested. These improved fits also reduce the significance of any residual around 2.1 keV.

We find consistent fits to the continuum parameters for MOS and PN data, as did B03/D L04.

We performed three different statistical analyses to test for the presence of a spectral feature in the region of 2.1 keV. All tests give consistent results and all tests indicate there is no third or fourth line.

We explicitly fit the spectral residuals at 2.1 keV. Using the continuum model favored by B03/D L04 we find that the statistically insignificant residuals in the PN singles spectrum occurs at the position of a Au-M edge. Our positioning of the residuals agrees with that obtained by fitting the known Au-M residuals in 3C 273 with an identical procedure. We further showed that the PN doublets events yield a misleadingly low energy for the residuals, and that when all the PN data is combined this shifts the residuals away from the Au-M edge position. This is highly suggestive of an instrumental origin for the insignificant residuals. In all eight physically plausible models, the residuals are always at the Au-M edge.

We have repeated the B03/D L04 analysis of 3C 273 to assess the effect of the Au-M edge in the 2.1 keV region. We find the EW of the residuals weaker relative to the 3C 273 than B03/D L04, and consistent with our other findings on significance of the residuals.

JC acknowledges financial support from NASA's Graduate Student Researchers Program NGT 5-50392. The authors thank Maurice Leutenegger for assistance and advice on various data processing issues.

APPENDIX

testing for a spectral line in a continuum

Some important results used in x4.2 are summarized here. The arguments of Eadie et al. (1983) are closely followed. Consider searching a region of interest (ROI) consisting of K bins for a deficit of counts over the expected continuum. The total spectrum has N bins. Define b_i as the true continuum, \hat{b}_i as the estimated continuum, and n_i as the observed counts in bin i . We can define the difference of counts in bin i as $s_i = n_i - \hat{b}_i$.

The search for residual in the K bins of the ROI can be formulated as a goodness-of-fit test, and under the null hypothesis H_0 there are no residuals, and $E(s_i) = E(n_i) - \hat{b}_i = b_i - \hat{b}_i = 0$, where E is the expectation (mean) operator. A reasonable test statistic is $T = \sum_{i=1}^K \frac{(n_i - \hat{b}_i)^2}{V(n_i - \hat{b}_i)}$ where $V()$ is the variance operator. This statistic is a function of the random variables $z_i = \frac{n_i - \hat{b}_i}{V(n_i - \hat{b}_i)}$.

The z_i have the following properties if H_0 is true. $E(z_i) = 0$, and $V(n_i - \hat{b}_i) = V(n_i) + V(\hat{b}_i) - \text{cov}(n_i; \hat{b}_i) = V(b_i) + V(\hat{b}_i) = \hat{b}_i + \gamma_i^2$. $\text{cov}()$ is the covariance operator. The trick is that the \hat{b}_i should be estimated using the $N - K$ bins outside the ROI, for then n_i and \hat{b}_i are uncorrelated and their covariance vanishes. The continuum is simply fit without utilizing the K bins in the ROI. Also note that $V(\hat{b}_i) = \gamma_i^2$ can be directly obtained from covariance matrix of

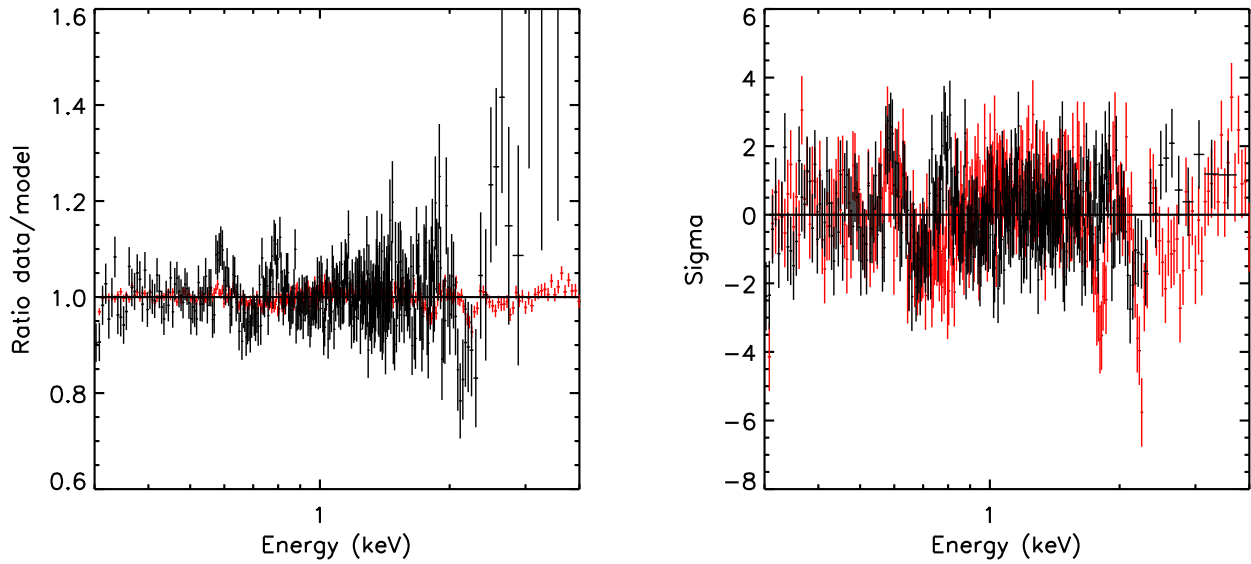


Fig. 10.1 Data/model ratio (left) and residuals (right) plot for 1E 1207 (black) and 3c273 (red).

the continuum. Thus under H_0 ,

$$T = \sum_{i=1}^K \frac{(n_i - \hat{b}_i)^2}{\hat{b}_i + \hat{\gamma}_i^2} = \sum_{i=1}^K z_i^2 \quad (A1)$$

and $E(z_i) = 0; V(z_i) = 1$. Thus the z_i are standard, normal variables (for s_i not too small), and $P(T)$ is a χ^2 distribution with K degrees of freedom.

For $K > 30$ we can simplify this result by defining a new statistic $y = \frac{T-K}{2K}$. Since the mean and variance of the χ^2 distribution are K and $2K$ respectively, y has a standard, normal distribution. Then as described in the text we can test H_0 by simply calculating y and if $y < y_c = 4$ we accept H_0 .

REFERENCES

Bevington, H. A. 1969, *Data Reduction and Error Analysis for the Physical Sciences* (New York: McGraw-Hill)

Bignami, G. F., Caraveo, P. A., Luca, A. D., & Mereghetti, S. 2003, *Nature*, 423, 725

De Luca, A., Mereghetti, S., Caraveo, P. A., Moroni, M., Mignani, R. P., & Bignami, G. F. 2004, *A&A*, 418, 625

Demmer, C. D. & Stumer, S. J. 1991, *ApJ*, 382, L23

Ende, W. T., Drijard, D., & James, F. E. 1983, *Statistical methods in experimental physics* (Amsterdam: North-Holland, 1983)

Giacani, E. B., Dubner, G. M., Green, A. J., Gross, W. M., & Gaisler, B. M. 2000, *AJ*, 119, 281

Haberl, F., Schweppe, A. D., Hammarayan, V., Hasinger, G., & Mutsch, C. 2003, *A&A*, 403, L19

Haberl, F., Zavlin, V. E., Trumper, J., & Burwitz, V. 2004, *A&A*, 419, 1077

Hailey, C. J. & Mori, K. 2002, *ApJ*, 578, L133

Ho, W. C. G. & Lai, D. 2003, *MNRAS*, 338, 233

Ho, W. C. G., Lai, D., Potekhin, A. Y., & Chabrier, G. 2003, *ApJ*, 599, 1293

Lampton, M., Margon, B., & Bowyer, S. 1976, *ApJ*, 208, 177

Mereghetti, S., De Luca, A., Caraveo, P. A., Becker, W., Mignani, R., & Bignami, G. F. 2002, *ApJ*, 581, 1280

Mori, K. & Hailey, C. J. 2003, submitted to *ApJ*, preprint (astro-ph/0301161)

Protassov, R., van Dyk, D. A., Connors, A., Kashyap, V. L., & Siemiginowska, A. 2002, *ApJ*, 571, 545

Roe, B. P. 1992, *Probability and Statistics in Experimental Physics*, Springer-Verlag, New York

Romani, R. W. 1987, *ApJ*, 313, 718

Rudemann, M. 2003, *Proceedings of the 4th AGILE Science Workshop*, preprint (astro-ph/0310777)

Rutledge, R. E., Bildsten, L., Brown, E. F., Pavlov, G. G., & Zavlin, V. E. 2002, *ApJ*, 577, 346

Sanwal, D., Pavlov, G. G., Zavlin, V. E., & Teter, M. A. 2002, *ApJ*, 574, L61

Sering, R. J. 1980, *Approximation Theorems of Mathematical Statistics* (New York: Wiley)

van Dyk, D. A., Connors, A., Kashyap, V. L., & Siemiginowska, A. 2001, *ApJ*, 548, 224

van Kerkwijk, M. H., Kaplan, D. L., Durant, M., Kulkarni, S. R., & Paerels, F. 2004, *ApJ*, 608, 432

Wang, F. Y. H., Rudemann, M., Halpern, J. P., & Zhu, T. 1998, *ApJ*, 498, 373

Zavlin, V. E., Pavlov, G. G., & Shibanov, Y. A. 1996, *A&A*, 315, 141

Zavlin, V. E., Pavlov, G. G., & Trumper, J. 1998, *A&A*, 331, 821

Table 1
Best-fit continuum parameters to PN data

	PN I(BB + BB)	PN II(BB + BB)	PN III(BB + BB)	PN I(HA + HA)	PN II(HA + HA)	PN III(HA + HA)
N_H [10^{22} cm $^{-2}$]	$0.126^{+0.017}_{-0.009}$	$0.128^{+0.017}_{-0.005}$	$0.132^{+0.012}_{-0.014}$	$0.146^{+0.009}_{-0.009}$	$0.151^{+0.010}_{-0.010}$	$0.155^{+0.007}_{-0.016}$
kT_S^1 [keV]	$0.159^{+0.009}_{-0.005}$	$0.154^{+0.010}_{-0.017}$	$0.153^{+0.015}_{-0.009}$	$0.116^{+0.009}_{-0.009}$	$0.109^{+0.006}_{-0.006}$	$0.116^{+0.009}_{-0.007}$
R_S^1 [km] ^a	$5.01^{+0.88}_{-0.36}$	$5.29^{+1.27}_{-0.54}$	$5.51^{+1.27}_{-0.72}$	$21.19^{+1.89}_{-3.73}$	$23.74^{+3.54}_{-2.45}$	$21.18^{+1.43}_{-3.90}$
kT_H^1 [keV]	$0.296^{+0.010}_{-0.012}$	$0.287^{+0.018}_{-0.020}$	$0.286^{+0.024}_{-0.010}$	$0.358^{+0.074}_{-0.057}$	$0.316^{+0.017}_{-0.040}$	$0.360^{+0.060}_{-0.064}$
R_H^1 [km] ^a	$0.97^{+0.13}_{-0.12}$	$1.09^{+0.19}_{-0.23}$	$1.10^{+0.19}_{-0.28}$	$0.68^{+0.40}_{-0.28}$	$1.01^{+0.54}_{-0.24}$	$0.67^{+0.72}_{-0.23}$
E_1 [keV]	$0.741^{+0.008}_{-0.006}$	$0.743^{+0.007}_{-0.007}$	$0.725^{+0.006}_{-0.005}$	$0.730^{+0.005}_{-0.005}$	$0.731^{+0.005}_{-0.005}$	$0.728^{+0.005}_{-0.005}$
1	$0.92^{+0.05}_{-0.07}$	$0.99^{+0.26}_{-0.10}$	$0.60^{+0.06}_{-0.03}$	$0.56^{+0.02}_{-0.02}$	$0.58^{+0.02}_{-0.01}$	$0.53^{+0.02}_{-0.03}$
$F_{W,H,M}$ [eV]	303^{+24}_{-26}	297^{+15}_{-22}	290^{+30}_{-20}	272^{+23}_{-18}	262^{+17}_{-16}	264^{+20}_{-19}
E_2 [keV]	$1.40^{+0.009}_{-0.010}$	$1.38^{+0.008}_{-0.009}$	$1.39^{+0.008}_{-0.008}$	$1.39^{+0.008}_{-0.008}$	$1.38^{+0.008}_{-0.008}$	$1.39^{+0.009}_{-0.008}$
2	$2.90^{+1.16}_{-1.16}$	$0.58^{+0.16}_{-0.10}$	$0.39^{+0.04}_{-0.02}$	$0.55^{+0.05}_{-0.07}$	$3.70^{+12.73}_{-1.97}$	$0.39^{+0.04}_{-0.04}$
$F_{W,H,M}$ [eV]	152^{+22}_{-102}	183^{+26}_{-13}	187^{+26}_{-25}	190^{+27}_{-24}	140^{+29}_{-52}	187^{+28}_{-23}
² -dof	0.98	0.98	0.99	0.98	0.98	0.98
dof	422	422	422	422	422	422

Note. | For hydrogen atmosphere models, we fixed neutron star mass and radius to $1.4 M_\odot$ and $10 \text{ km} \cdot \text{km}^{-1}$ and R^1 are insensitive to variation of M and R (Zavlin et al. 1998).

^aFor apparent radius, we assumed distance is 2.1 kpc and the error bars do not include uncertainty in distance. The distance to the supernova remnant PKS 1209-51 was measured to be 2.1 kpc (Giacani et al. 2000).

Table 2
Best-fit continuum parameters to MOS data

Instrument	MOS1	MOS1	MOS2	MOS2
Model	III(BB + BB)	III(HA + HA)	III(BB + BB)	III(HA + HA)
N_H [10^{22} cm $^{-2}$]	$0.053^{+0.105}_{-0.041}$	$0.176^{+0.035}_{-0.037}$	$0.075^{+0.074}_{-0.053}$	$0.182^{+0.011}_{-0.050}$
kT_S^1 [keV]	$0.197^{+0.026}_{-0.027}$	$0.117^{+0.025}_{-0.016}$	$0.204^{+0.021}_{-0.030}$	$0.123^{+0.018}_{-0.020}$
R_S^1 [km]	$3.44^{+1.54}_{-1.16}$	$20.27^{+9.76}_{-7.73}$	$2.95^{+1.55}_{-0.78}$	$18.06^{+18.62}_{-6.07}$
kT_H^1 [keV]	$0.374^{+0.074}_{-0.040}$	$0.407^{+0.107}_{-0.057}$	$0.373^{+0.056}_{-0.039}$	$0.418^{+0.083}_{-0.063}$
R_H^1 [km]	$0.389^{+0.27}_{-0.17}$	$0.49^{+0.46}_{-0.20}$	$0.374^{+0.38}_{-0.17}$	$0.43^{+0.59}_{-0.17}$
E_1 [keV]	$0.700^{+0.033}_{-0.031}$	$0.728^{+0.013}_{-0.016}$	$0.718^{+0.018}_{-0.046}$	$0.729^{+0.013}_{-0.016}$
1	$0.90^{+0.52}_{-0.22}$	$0.62^{+0.12}_{-0.05}$	$0.68^{+0.12}_{-0.12}$	$0.56^{+0.09}_{-0.06}$
$F_{W,H,M}$ [eV]	429^{+216}_{-85}	330^{+43}_{-31}	392^{+146}_{-61}	319^{+56}_{-37}
E_2 [keV]	$1.42^{+0.009}_{-0.010}$	$1.42^{+0.009}_{-0.009}$	$1.40^{+0.010}_{-0.009}$	$1.40^{+0.009}_{-0.009}$
2	$0.46^{+0.04}_{-0.05}$	$0.39^{+0.05}_{-0.05}$	$0.47^{+0.05}_{-0.05}$	$0.44^{+0.04}_{-0.04}$
$F_{W,H,M}$ [eV]	236^{+43}_{-38}	181^{+35}_{-30}	229^{+35}_{-37}	215^{+34}_{-31}
² -dof	0.85	0.80	1.20	1.18
dof	139	139	137	137

Table 3
Effects of spectral binning on χ^2 and χ^2_{ν} .

dof	χ^2	χ^2_{ν}
422	0.98	31.8
358	1.05	32.7
235	1.11	32.3
131	1.33	31.1
81	1.43	32.6
94	1.8	60

Note. | We adopt continuum model III(BB + BB) to fit PN-single data. The last line shows the results of DL04.

Table 4
Goodness-of-fit parameters of 3rd line test

Continuum model	Parameters	PN single	PN double	MOS1	MOS2
III(BB + BB)	T_c	112.8	71.38	65.26	65.26
	T	85.90	43.42	24.79	41.03
	1 C	1.7 $\times 10^{-2}$	5.4 $\times 10^{-2}$	5.3 $\times 10^{-1}$	3.1 $\times 10^{-2}$
III(HA + HA)	T_c	112.8	71.38	65.26	65.26
	T	80.45	42.62	20.47	34.68
	1 C	3.3 $\times 10^{-2}$	6.3 $\times 10^{-2}$	7.7 $\times 10^{-1}$	1.2 $\times 10^{-1}$

Note. | Model I and II show very similar results as model III.

Table 5
Summary statistics for 3rd feature significance

Instrument	Continuum model	P (F) analysis ^a	Goodness-of-fit test ^{a,b}	EW analysis ^{a,b}
PN-single	I (BB *L3+ BB)	1.77	2.13	*
	I (BB + BB *L3)	3.29	2.13	2.07
	I (HA *L3+ HA)	2.81	1.18	1.69
	I (HA + HA *L3)	2.84	1.18	1.96
	II (BB + BB *L3)	3.27	2.22	2.18
	II (HA + HA *L3)	2.55	1.69	1.85
	III (BB + BB)*L3	3.26	2.17	2.14
	III (HA + HA)*L3	3.12	1.83	1.88
MOS1	I (BB *L3+ BB)	0.70	0.33	*
	I (BB + BB *L3)	2.09	0.33	1.92
	I (HA *L3+ HA)	0.32	-0.92	#
	I (HA + HA *L3)	0.32	-0.92	#
	II (BB + BB *L3)	2.36	0.28	1.82
	II (HA + HA *L3)	1.02	-0.83	#
	III (BB + BB)*L3	2.55	-0.07	1.36
	III (HA + HA)*L3	1.32	-0.73	#
MOS2	I (BB *L3+ BB)	0.69	1.78	*
	I (BB + BB *L3)	2.21	1.78	1.65
	I (HA *L3+ HA)	0.27	1.05	#
	I (HA + HA *L3)	-1.43	1.05	#
	II (BB + BB *L3)	2.17	1.97	1.68
	II (HA + HA *L3)	1.14	1.37	#
	III (BB + BB)*L3	2.14	1.87	1.87
	III (HA + HA)*L3	1.11	1.18	#

^aThe units of significance are sigma.

^bThese results have not been corrected for blind search. This will reduce the significance of the results (see x4).

Low temperature continuum too weak to determine EW (see x4.3)

The residuals in this case were essentially non-existent (see x4.3)